GALCIT REPORT NO. 221

683

GUGGENHEIM AERONAUTICS LABORATORY

CALIFORNIA INSTITUTE OF TECHNOLOGY

ADDITIONAL WIND TUNNEL TESTS ON A 1/14TH SCALE MODEL OF THE CONSOLIDATED XPB2Y-1 FLYING BOAT, WITH PARTICULAR REGARD TO TAIL SURFACES

REPORT 221

CONFIDENTIAL

GUGGENHEIM AERONAUTICS LABORATORY

CALIFORNIA INSTITUTE OF TECHNOLOGY

PASADENA

REPORT ON

ADDITIONAL WIND TUNNEL TESTS ON A 1/14TH SCALE MODEL OF THE CONSOLIDATED XPB2Y-1 FLYING BOAT, WITH PARTICULAR REGARD TO TAIL SURFACES

PREPARED BY

William R. Sears

No. of pages 155

No. of figures 108

No. of photographs 14

Date December 1, 1938

Wind Tunnel Section

RUN	CONFIGURATION	TEST	$\frac{g}{gm/cm^2}$	ADJUSTMENTS (DEG)	REMARKS
1	$WBN_cPH_3V_3$	Y	35	$\alpha_u=3$, $r=0$	
2	$WBN_cPH_2V_2v$	"	"	" "	
3	"	"	"	" , r = FREE	
4	$WBN_cPH_3V_3$	"	"	" "	
5	WBN_cPH_3	"	"	"	
6	WBN_cPH_3v	"	"	"	
7	WBN_cP	"	"	"	
8	$WBN_cPH_2V_4v$	"	"	" , $r=0$	
9	WBN_cPH_2bv	"	"	"	
10	WBN_cPH_2b	"	"	"	
11	$WBN_cPH_3V_3$	RUD. H.M.	"	" , $\psi=10$, $r_t=0$, RIGHT RUD. ONLY	
12	"	"	"	" , $\psi=-5$, " , "	
13	"	"	"	" , $\psi=0$, " , "	
14	"	"	"	" , $\psi=5$, " , "	
15	"	"	"	" , $\psi=10$, " , "	
16	"	"	"	" , $\psi=0$, $r_t=-5$, "	
17	"	"	"	" , " , $r_t=-10$, "	
18	"	"	"	" , " , $r_t=-20$, "	
19	"	Y	"	" , $r=-5$, $r_t=0$	
20	"	"	"	" , $r=-10$, "	
21	"	"	"	" , $r=-20$, "	RUDDER SLIPPED DURING RUN
22	"	"	"	" , $r_l=5$, $r_r=-5$	
23	$WBN_cPH_3V_5$	RUD. H.M.	"	" , $\psi=0$, $r_t=0$, RIGHT RUD. ONLY	
24	"	"	"	" , $\psi=-5$, " , "	
25	"	"	"	" , $\psi=-10$, " , "	
26	$WBN_cPH_2V_2v$	"	"	" , $\psi=0$, $r_t=0$	
27	"	"	"	" , $\psi=-5$, "	
28	"	"	"	" , $\psi=-10$, "	
29	$WBN_cPH_2V_1v$	"	"	" , $\psi=0$, "	
30	"	"	"	" , $\psi=-5$, "	
31	"	"	"	" , $\psi=-10$, "	

RUN	CONFIGURATION	TEST	q $\frac{gm}{cm^2}$	ADJUSTMENTS (DEG)	REMARKS
32	$WBN_cPH_3V_6$	Y	35	$\alpha_u=3$, $r=0$	
33	WBP	MDP	"		TAIL REMOVED AT STABILIZER
34	WBN_cP	"	"		
35	$WBN_cPH_3V_3$	"	"	$\delta=3$, $e=0$, $e_1=0$	
36	"	P	"	$\delta=-1$, $e=e_1=e_t=0$	
37	"	"	"	" , $e=-3$, $e_1=e_t=0$	
38	"	"	"	" , $e=3$, "	
39	"	"	"	" , $e=6$, "	
40	"	"	"	" , $e=10$, "	
41	"	"	"	" , $e=15$, "	
42	"	"	"	" , $e=-15$, $e_1=-15$, $e_t=0$	
43	"	"	"	" , " , $e_1=0$, "	
44	"	ELEV. H.M.	"	" , $e_t=0$, $\alpha_u=2.8$	
45	"	"	"	" , " , $\alpha_u=12°$	
46	"	"	"	" , " , $\alpha_u=2.8$ AND 12	H.M. OF $e+e_1$
47	$WBPN_cH_3V_3F^{40}$	"	"	" , " , $\alpha_u=12$	
48	$WBPH_3V_3$	"	"	" , " , "	
49	$WBPN_cH_3V_3$	"	"	" , " , $\alpha_u=7$	
50	"	"	"	" , $e_t=-5$, $\alpha_u=2.8$	
51	"	"	"	" , " , $\alpha_u=7$	
52	"	"	"	" , $e_t=5$, $\alpha_u=2.8$	
53	"	"	"	" , $e_t=10$, "	
54	"	"	"	" , $e_t=20$, "	
55	"	"	"	" , $e_t=-\frac{1}{2}e$, "	
56	"	"	"	" , " , $\alpha_u=12$	
57	"	"	"	" , $e_t=-\frac{1}{3}e$, "	
58	"	"	"	" , " , $\alpha_u=2.8$	
59	"	"	"	" , $e_t=-e$, "	
60	"	P	"	" , e_{FREE}, $e_t=-\frac{1}{3}e$	
61	"	"	"	" , " , $e_t=-\frac{1}{2}e$	

RUN	CONFIGURATION	TEST	q gm/cm²	ADJUSTMENTS (DEG.)	REMARKS
62	$WBPN_c H_3 V_3 F^{40}$	P	35	$\delta=-1$, e FREE, $e_t=-\frac{1}{2}e$	
63	"	"	"	" , " , $e_t=-\frac{1}{3}e$	
64	"	"	"	" , " , $e_t=0$	
65	$WBPN_c H_3 V_3$	"	"	" , " , "	
66	"	"	"	" , " , $e_t=5$	
67	"	"	"	" , $e=-6$, $e_t=0$	
68	"	"	"	" , $e=-10$, "	
69	$WBPN_c H_3 V_3 F^{40}$	"	"	" , " , "	
70	"	"	"	" , $e=-15$, "	
71	"	"	"	" , " , $e_1=-15$	
72	"	"	"	" , $e=-20$, $e_1=-20$	
73	"	"	"	" , " , $e_1=0$	
74	$WBPN_c H_3 V_3$	"	"	" , " , "	
75	"	"	"	" , " , $e_1=-20$	
76	$WBPN_c H_3 V_3 F^{40}$	"	"	" , $e=0$, $e_1=0$	
77	$WBPN_c H_3 V_3$	"	"	$\delta=-3.5$, " , "	
78	$WBPN_c H_2 V_2 v$	M.D.P.	"	$\delta=-1$, "	
79	"	ELEV. H.M.	"	" , $e_t=0$, $\alpha_u=2.8$	
80	"	"	"	" , " , $\alpha_u=7$	
81	"	"	"	" , " , $\alpha_u=12$	
82	$WBPN_c H_2 V_2 v F^{40}$	"	"	" , " , "	
83	"	"	"	" , " , $\alpha_u=7$	
84	"	"	"	" , " $\alpha_u=2.8$	
85	$WBPN_c H_2 V_2 v$	"	"	" , $e_t=-5$, $\alpha_u=7$	
86	"	"	"	" , $e_t=5$, α "	
87	"	"	"	" , $e_t=10$, "	
88	"	"	"	" , $e_t=-10$, "	
89	$WBPN_c H_1 V_2 v$	P	"	" , $e_t=0$, e FREE	
90	$WBPN_c H_1 V_2 v F^{40}$	"	"	" , " , "	
91	$WBPN_c H_1 V_2 v$	"	"	" , $e_t=-.3e+2.5$, "	
92	"	"	"	" $e_t=-.3e+5$, "	

RUN	CONFIGURATION	TEST	q gm/cm²	ADJUSTMENTS (DEG.)	REMARKS
93	$WBPN_c H_1 V_2 v$	ELEV. H.M.	35	$\delta=-1$, $e_t=0$, $\alpha_u=2.8$	
94	"	"	"	" , " , $\alpha_u=7$	
95	"	"	"	" , " , $\alpha_u=12$	
96	"	"	"	" , $e_t=-0.3e$, $\alpha_u=2.8$	
97	"	"	"	" , " , $\alpha_u=7$	
98	"	"	"	" , " , $\alpha_u=12$	
99	"	P	"	" , " , e FREE	
100	$WBPN_c H_4 V_3 v$	"	"	" , $e_t=0$, "	FLUTTER - NO DATA TAKEN
101	"	H.M.	"	" , "	" " " "
102	$WBPN_c H_2 V_2 v$	P	"	" , " , e FREE	
103	$WBPN_c H_2 V_2 v F^{40}$	"	"	" , " , "	
104	$WBPN_c H_2 V_2 v$	"	"	" , $e_t=2.5$, "	
105	"	"	"	" , $e_t=5$, "	
106	"	"	"	" , $e_t=0$, $e=-5$	
107	"	"	"	" , " , $e=-10$	
108	"	"	"	" , " , $e=-15$	
109	"	"	"	" , " , $e=-20$	
110	$WBPN_c H_2 V_2 v M$	MDP	"	" , " , $e=0$	
111	$WBPN_c H_2 V_2 v F^{20}$	P	"	" , " , "	
112	$WBPN_c H_2 V_2 v F^{40}$	"	"	" , " , "	
113	$WBPN_c H_2 V_2 v$	ELEV. H.M.	"	" , " , $\alpha_u=7$	
114	"	"	"	" , " , $\alpha_u=9$	
115	"	"	"	" , " , $\alpha_u=11$	
116	"	"	"	$\delta=1.7$, " , $\alpha_u=7$	,
117	"	P	"	" , $e=0$	
118	$WBPN_c F^{40}$	"	"		TAIL REMOVED AT DECK LINE
119	$WBPN_c H_5 V_3$	ELEV H.M	"	$\delta=-1$, $e_t=0$, $\alpha_u=2.8$	
120	"	"	"	" , " , $\alpha_u=7$	
121	"	"	"	" , " , $\alpha_u=12$	
122	"	"	"	" , " , $\alpha_u=20$	

RUN	CONFIGURATION	TEST	q gm/cm²	ADJUSTMENTS (DEG)	REMARKS
123	$WBPN_c H_5 V_3$	P	35	$\delta=-1$, $e_t=0$, e FREE	
124	"	"	"	" , " , $e=0$	
125	"	"	"	" , " , $e=-5$	
126	"	"	"	" , " , $e=-10$	
127	$WBPN_c H_6 V_3$	ELEV. H.M.	"	" , " , $\alpha_u=2.8$	
128	"	"	"	" , " , $\alpha_u=7$	
129	"	"	"	" , " , $\alpha_u=12$	
130	"	P	"	" , " , e FREE	
131	"	"	"	" , " , $e=0$	
132	"	"	"	" , " , $e=-5$	
133	"	"	"	" , " , $e=-10$	
134	"	"	"	" , " , $e=-15$	
135	"	ELEV. H.M.	"	" , " , $\alpha_u=2.8$	ELEV. GAP OPEN-.11 IN.
136	"	"	"	" , " , $\alpha_u=7$	" " " "
137	"	"	"	" , " , $\alpha_u=12$	" " " "
138	"	P	"	" , " , e FREE	" " " "
139	"	"	"	" , " , $e=0$	" " " "
140	"	"	"	" , " , $e=-10$	" " " "
141	$WBPN_c H_7 V_3$	ELEV. H.M.	"	" , " , $\alpha_u=2.8$	
142	"	"	"	" , " , $\alpha_u=7$	
143	"	"	"	" , " , $\alpha_u=12$	
144	"	P	"	" , " , e FREE	
145	"	"	"	" , " , $e=0$	
146	"	"	"	" , " , $e=-10$	
147	"	"	"	" , " , $e=-20$	
148	$WBPN_c H_8 V_3$	ELEV. H.M.	"	" , " , $\alpha_u=2.8$	HINGE MOMENT WIRES REMAIN ON FOR ALL RUNS FROM HERETO 167
149	"	"	"	" , " , $\alpha_u=7$	
150	"	"	"	" , " , $\alpha_u=12$	
151	"	P	"	" , " , e FREE	
152	$WBPN_c H_8 V_3 F^{40}$	"	"	" , " , "	

RUN	CONFIGURATION	TEST	q gm/cm²	ADJUSTMENTS (DEG.)	REMARKS
153	$WBPN_c H_8 V_3 F^{40}$	ELEV H.M.	35	$\delta=-1$, $e_t=0$, $\alpha_u=2.8$	
154	"	HMP	"	" , " , $\alpha_u=7$	
155	"	"	"	" , " , $\alpha_u=12$	
156	"	ELEV. H.M.	"	" , " , " , $e=e_1$	
157	$WBPN_c H_8 V_3$	"	"	" , " , " , "	
158	"	"	"	" , $e_t=-5$, $\alpha_u=2.8$	
159	"	"	"	" , $e_t=10$, "	
160	"	"	"	" , $e_t=20$, "	
161	"	"	"	" , $e_t=5$, "	
162	"	P	"	" , " , e_{FREE}	
163	"	"	"	" , $e_t=-\frac{1}{3}e$, "	
164	"	"	"	" , $e_t=-\frac{1}{2}e$, "	
165	"	ELEV. H.M.	"	" , " , $\alpha_u=2.8$	
166	"	"	"	" , $e_t=-\frac{1}{3}e$, "	
167	"	P	"	" , $e_t=0$, $e=0$	
168	$WBPN_c H_8 V_3 F^{40}$	"	"	" , " , "	
169	$WBPN_c H_8 V_3$	"	"	" , " , $e=5$	
170	"	"	"	" , " , $e=-5$	
171	"	"	"	" , " , $e=-10$	
172	$WBPN_c H_8 V_3 F^{40}$	"	"	" , " , "	
173	"	"	"	" , " , $e=e_1=-10$	
174	$WBPN_c H_8 V_3$	"	"	" , " , "	
175	"	"	"	" , " , $e=-15$	
176	$WBPN_c H_8 V_3 F^{40}$	"	"	" , " , "	
177	"	"	"	" , " , $e=-20$	
178	$WBPN_c H_8 V_3$	"	"	" , " , "	
179	"	"	"	" , " , $e=e_1=-20$	
180	$WBPN_c H_8 V_3 F^{40}$	"	"	" , " , "	
181	"	"	"	" , " , $e=-25$	
182	$WBPN_c H_8 V_3$	"	"	" , " , "	

RUN	CONFIGURATION	TEST	q gm/cm²	ADJUSTMENTS (DEG)	REMARKS
183	$WBPN_cH_8V_3$	ELEV. H.M.	35	$\delta=-1$, $e_t=0$, $\alpha_u=2.8$, $r=10$	
184	"	"	"	" , " , $\alpha_u=7$, "	
185	"	"	"	" , " , " , $r=0$	CHECK ON RUN 149
186	"	"	"	" , " , $\alpha_u=2.8$, "	" " " 148
187	"	"	"	" , $e_t=-10$, $\alpha_u=7$	
188	"	"	"	" , $e_t=10$, "	
189	"	"	"	" , $e_t=20$, "	
190	$WBPN_cH_9V_3$	HMP	"	" , $e_t=0$, $\alpha_u=2.8$	
191	"	"	"	" , " , $\alpha_u=6$	
192	"	"	"	" , " , $\alpha_u=9$	
193	"	"	"	" , " , $\alpha_u=12$	
194	"	P	"	" , " , e_{FREE}	
195	$WBPN_cH_9V_3F^{40}$	HMP	"	" , " , $\alpha_u=2.8$	
196	"	"	"	" , " , $\alpha_u=6$	
197	"	"	"	" , " , $\alpha_u=9$	
198	"	P	"	" , " , e_{FREE}	
199	"	ELEV. H.M.	"	" , $e_t=10$, $\alpha_u=9$	
200	$WBPN_cH_9V_3$	"	"	" , " , "	
201	"	"	"	" , $e_t=15$, "	
202	$WBPN_cH_9V_3F^{40}$	"	"	" , " , "	
203	$WBPN_cH_{10}V_3$	HMP	"	" , $e_t=0$, $\alpha_u=2.8$	
204	"	"	"	" , " , $\alpha_u=6$	
205	"	"	"	" , " , $\alpha_u=9$	
206	"	"	"	" , " , $\alpha_u=12$	
207	"	P	"	" , " , e_{FREE}	
208	$WBPN_cH_{11}V_3$	HMP	"	" , " , $\alpha_u=2.8$	
209	"	ELEV. H.M.	"	" , " , $\alpha_u=6$	
210	"	"	"	" , " , $\alpha_u=9$	
211	"	HMP	"	" , " , $\alpha_u=12$	
212	"	P	"	" " , e_{FREE}	

RUN	CONFIGURATION	TEST	$\frac{q}{gm/cm^2}$	ADJUSTMENTS (DEG)	REMARKS
213	$WBPN_c H_{12} V_3$	ELEV. H.M.	35	$\delta=-1$, $e_t=0$, $\alpha_u=2.8$	
214	"	"	"	" , " , $\alpha_u=6$	
215	"	"	"	" , " , $\alpha_u=9$	
216	"	"	"	" , " , $\alpha_u=12$	
217	$WBPN_c H_2 V_2 V+6$	"	"	" , " , $\alpha_u=7$	
218	"	"	"	" , " , $\alpha_u=9$	
219	"	"	"	" , " , $\alpha_u=11$	
220	"	"	"	" , " , $\alpha_u=2.8$	
221	$WBPN_c H_2 V_2 F^{40}$	P	"	" , " , $e=0$	
222	"	"	"	" , " , $e=-10$	
223	"	"	"	" , " , $e=-15$	
224	"	"	"	" , " , $e=-20$	
225	"	ELEV. H.M.	"	" , $e_t=-5$, $\alpha_u=7$	
226	"	"	"	" , " , $\alpha_u=10$	
227	$WBPN_c F^{20}$	P	"		TAIL REMOVED AT DECK LINE
228	$WBPN_c$	"	"		" " " " "
229	"	AIL. H.M.	"	$\alpha_u=2.8$	
230	"	"	"	$\alpha_u=6$	
231	"	"	"	$\alpha_u=9$	
232	"	"	"	$\alpha_u=12$	
233	$WBPN_c H_{13} V_3$	HMP	"	$\delta=-1$, $e_t=0$, $\alpha_u=2.8$	
234	$WBPN_c H_{14} V_3$	"	"	" , " , "	
235	$WBPN_c H_{15} V_3$	"	"	" , " , "	
236	"	"	"	" , " , $\alpha_u=5$	
237	"	"	"	" , " , $\alpha_u=7.5$	
238	"	"	"	" , " , $\alpha_u=10$	
239	"	"	"	" , " , $\alpha_u=12$	
240	$WBPN_c H_{16} V_3$	"	"	" , " , $\alpha_u=2.8$	
241	"	"	"	" , " , $\alpha_u=5$	
242	$WBPN_c H_{17} V_3$	ELEV. H.M.	"	" , " , $\alpha_u=2.8$	

RUN	CONFIGURATION	TEST	q gm/cm²	ADJUSTMENTS (DEG.)	REMARKS
243	$WBPN_c H_{16} V_3$	HMP	35	$\alpha = -1$, $e_t = 0$, $\alpha_u = 7.5$	
244	"	"	"	" , " , $\alpha_u = 10$	
245	"	"	"	" , " , $\alpha_u = 12$	
246	"	P	"	" , " , e FREE	
247	$WBPN_c H_{16} V_3 F^{40}$	HMP	"	" , " , $\alpha_u = 2.8$	
248	"	"	"	" , " , $\alpha_u = 5$	
249	"	"	"	" , " , $\alpha_u = 7.5$	
250	"	"	"	" , " , $\alpha_u = 10$	
251	"	P	"	" , " , e FREE	
252	"	ELEV H.M.	"	" , $e_t = -10$, $\alpha_u = 10$	
253	$WBPN_c H_{16} V_3$	"	"	" , " , $\alpha_u = 2.8$	
254	"	"	"	" , " , $\alpha_u = 12$	
255	"	"	"	" , $e_t = 10$, $\alpha_u = 2.8$	
256	"	"	"	" , " , $\alpha_u = 12$	
257	$WBPN_c H_{16} V_3 F^{40}$	"	"	" , " , $\alpha_u = 10$	
258	"	"	"	" , $e_t = 20$, "	
259	$WBPN_c H_{16} V_3$	"	"	" , " , $\alpha_u = 2.8$	
260	"	"	"	" , " , $\alpha_u = 12$	
261	$WBPN_c H_{16} V_3 + G$	"	"	" , $e_t = 0$, $\alpha_u = 6$	
262	$WBPN_c H_2 V_2' v$	HMY	"	$\alpha_u = 3°$, $r_t = 0$, $\psi = 0$	
263	"	"	"	" , " , $\psi = -2.5$	
264	"	"	"	" , " , $\psi = -5$	
265	"	"	"	" , " , $\psi = -7.5$	
266	"	"	"	" , " , $\psi = -10$	
267	"	"	"	" , " , $\psi = -15$	
268	"	"	"	" , " , $\psi = 2.5$	
269	"	Y	"	" , " , RUDDER FREE	
270	$WBPN_c H_{16} V_3$	HMY	"	" , " , $\psi = 0$	WIRES CONNECTING RUDDERS
271	"	"	"	" , " , $\psi = -5$	" " "
272	"	Y	"	" , " , RUDDER FREE	WIRES ATTACHED

RUN	CONFIGURATION	TEST	q gm/cm²	ADJUSTMENTS (DEG.)	REMARKS
273	$WBPN_c H_{16} V_3$	HMY	35	$\alpha_u = 3$, $r_t = 0$, $\psi = 2.5$	STRUT CONNECTING RUDDERS IN RUNS 273-323 INCL
274	"	"	"	" , " , $\psi = 0$	
275	"	"	"	" , " , $\psi = -2.5$	
276	"	"	"	" , " , $\psi = -5$	
277	"	"	"	" , " , $\psi = -7.5$	
278	"	"	"	" , " , $\psi = -10$	
279	"	"	"	" , " , $\psi = -15$	
280	"	Y	"	" , " , RUDDER FREE	
281	"	"	"	" , " , " FIXED	
282	"	RUD HM	"	" , $r_t = -20$, $\psi = 0$	
283	"	"	"	" , " , $\psi = -10$	
284	"	"	"	" , $r_t = -10$, $\psi = 0$	
285	"	"	"	" , " , $\psi = -10$	
286	"	"	"	" , $r_t = 12$, $\psi = 0$	
287	"	"	"	" , " , $\psi = -10$	
288	"	Y	"	" , $r_t = -\frac{2}{3} r$, RUDDER FREE	
289	"	RUD. HM.	"	" , " , $\psi = 0$	
290	"	"	"	" , " , $\psi = -2.5$	
291	"	"	"	" , " , $\psi = -5$	
292	"	"	"	" , " , $\psi = -7.5$	
293	"	"	"	" , " , $\psi = -10$	
294	"	Y	"	" , $r_t = -r$, RUDDER FREE	
295	"	RUD HM	"	" , " , $\psi = 0$	
296	"	HMY	"	" , $r_t = -\frac{2}{3} r$, "	
297	$WBPN_c H_{16} V_6$	Y	"	" , " , RUDDER FREE	
298	$WBPN_c H_{16} V_7$	HMY	"	" , $r_t = 0$, $\psi = 2.5$	
299	"	"	"	" , " , $\psi = 0$	
300	"	"	"	" , " , $\psi = -2.5$	
301	"	"	"	" , " , $\psi = -5$	
302	"	"	"	" , " , $\psi = -7.5$	

RUN	CONFIGURATION	TEST	q gm/cm²	ADJUSTMENTS (DEG)	REMARKS
303	$WBPN_c H_{16} V_7$	HMY	35	$\alpha_u = 3$, $r_t = 0$, $\Psi = -10$	
304	"	"	"	" , " , $\Psi = -15$	
305	"	Y	"	" , " , RUDDER FREE	
306	$WBPN_c H_{16} V_8$	"	"	" , " , " "	
307	$WBPN_c H'_{16} V_8$	"	"	" , " , " "	
308	$WBPN_c H_{16} V_9$	"	"	" , " , " "	
309	"	HMY	"	" , " , $\Psi = 2.5$	
310	"	"	"	" , " , $\Psi = 0$	
311	"	"	"	" , " , $\Psi = -2.5$	
312	"	"	"	" , " , $\Psi = -5$	
313	"	"	"	" , " , $\Psi = -7.5$	
314	"	"	"	" , " , $\Psi = -10$	
315	"	"	"	" , " , $\Psi = -15$	
316	$WBPN_c H_{16} V_{10}$	Y	"	" , " , RUDDER - FREE	
317	"	HMY	"	" , " , $\Psi = 2.5$	
318	"	"	"	" , " , $\Psi = 0$	
319	"	"	"	" , " , $\Psi = -2.5$	
320	"	"	"	" , " , $\Psi = -5$	
321	"	"	"	" , " , $\Psi = -7.5$	
322	"	"	"	" , " , $\Psi = -10$	
323	"	"	"	" , " , $\Psi = -15$	
324	$WBPN_c F_2$	Y	"		
325	$WBPN_c H_2 V_2'' v$	"	"	$\alpha_u = 3$, $r_t = 0$, RUDDER - FREE	
326	"	HMY	"	" , " , $\Psi = 2.5$	
327	"	"	"	" , " , $\Psi = 0$	
328	"	"	"	" , " , $\Psi = -2.5$	
329	"	"	"	" , " , $\Psi = -5$	
330	"	"	"	" , " , $\Psi = -7.5$	
331	"	"	"	" , " , $\Psi = -10$	
332	"	"	"	" , " , $\Psi = -15$	

RUN	CONFIGURATION	TEST	q $\frac{gm}{cm^2}$	ADJUSTMENTS (DEG.)	REMARKS
333	WB, P	MDP	35		
334	WB, PN_c	"	"		
335	WB, $PN_c H_{18} V_{11}$	"	"	$\delta = -2$	
336	"	"	"	$\delta = -1$	
337	WB, $PN_c H_{18} V_{11} M_3$	MD	"	"	TAIL REMOVED AT STAB. ON ALL SUBSEQUENT RUNS
338	WB, $PN_c H_{18} V_{11} M_3^F$	"	"	"	
339	WB, $PN_c H_{18} V_{11}$	ELEV H.M.	"	" , $\alpha_u = 4$, $e_t = 20$	
340	"	"	"	" , " , $e_t = 15$	
341	"	"	365	" , " , $e_t = 10$	
342	"	"	"	" , " , $e_t = -10$	
343	"	HMP	35	" , $\alpha_u = 0$, $e_t = 0$	
344	"	"	"	" , $\alpha_u = 2$, "	
345	"	"	"	" , $\alpha_u = 4$, "	
346	"	"	"	" , $\alpha_u = 6$, "	
347	"	"	"	" , $\alpha_u = 8$, "	
348	"	"	"	" , $\alpha_u = 10$, "	
349	"	"	"	" , $\alpha_u = 12$, "	
350	WB, $PN_c H_{18} V_{11} F^{40}$	"	"	" , $\alpha_u = 6$, "	
351	"	"	"	" , $\alpha_u = 8$, "	
352	"	"	"	" , $\alpha_u = 10$, "	
353	WB, $PN_c H_{19} V_{11}$	"	"	" , $\alpha_u = 2$, "	
354	"	"	"	" , $\alpha_u = 6$, "	
355	"	"	"	" , $\alpha_u = 10$, "	
356	"	"	"	" , $\alpha_u = 12$, "	
357	WP + SINGLE FLOAT	MDP	"	$\iota = 1°$	
358	WP	"	"		
359	WB_2P	"	"		
360	WB_2P + FAIRING	MD	"		FAIRING — PHOTOS 11, 12
361	WB_2PK	"	"		
362	WB_2PKM_4	"	"		

RUN	CONFIGURATION	TEST	q gm/cm^2	ADJUSTMENTS (DEG.)	REMARKS
363	$WB_2PKM_4N_2$	MDP	35		
364	$WB_2PKM_4N_2H_{18}V_{11}$	"	"	$\delta=-1$	
365	WB_2PN_2	Y	"	$i=3$ REL WING, $a_u=3$	
366	$WB_2PN_2H_{18}V_{11}$	"	"	$\delta=-1$, $a_u=3$	
367	$WB_2PN_2H_{18}V_{11}KM_4$	"	"	" , "	
368	"	VELOCITY MEASURE	"	$2\frac{1}{2}$" ABOVE H	PITOT 51¼" AFT OF BRACE STRUT
369	"	"	"	$8\frac{1}{2}$" " "	" 48¼" " "
370	"	"	"	PITOT $4\frac{5}{8}$" IN FRONT OF LEFT RUDDER	
371	WB_1PN_c	Y	"		
372	$WB_1PN_cH_{18}V_{11}$	"	"	$\delta=-1$, $r=0$	
373	$WB_1PN_cH_{18}V_{11}M_3$	"	"	" , "	
374	$WB_1PN_cH_{18}V_{11}$	RUD H.M.	"	" , $r_t=20$, $\psi=0$	STRUT CONNECTING RUDDERS
375	"	"	"	" , $r_t=-20$, "	" "
376	"	"	"	" , $r_t=-10$, "	" "
377	"	"	"	" , $r_t=10$, "	" "
378	"	HMY	"	" , $r_t=0$, $\psi=5$	" "
379	"	"	"	" , " , $\psi=2.5$	" "
380	"	"	"	" , " , $\psi=0$	" "
381	"	"	"	" , " , $\psi=-2.5$	" "
382	"	"	"	" , " , $\psi=-5$	" "
383	"	"	"	" , " , $\psi=-10$	" "
384	"	"	"	" , " , $\psi=-15$	" "
385	STATIC H.M. WITH V_{11} OFF AND WIND ON AND OFF, $q=35$				

DEFINITIONS OF RUNS

P ⟷ POLAR

M.D. ⟷ MINIMUM-DRAG-REGION POLAR

Y ⟷ YAWING MOMENTS AT ANGLES OF YAW

H.M. ⟷ HINGE MOMENT

LIST OF FIGURES

1. Three-view of Consolidated XP2Y-1 (as flown), configuration $B_1P_1H_1H_2V_2$
2. Three-view of Consolidated XP2Y-1 (proposed production model), configuration $B_2P_2H_4H_5H_{10}V_{11}$
3. [illegible]
4. Hulls B, B_1, fairing F_2, turret T
4a. Gun turret T_3
5. Hull B_2, turrets T and T_4
6. Nacelles N and N_0
7. Nacelle N_2
8. Horizontal tails H_1 and H_2
9. Twin tail H_3
10. Stabilizer and rudder profiles in H_1, H_2, H_3, H_4, H_5, H_6
11. Stabilizer and rudder profiles in H_6 + 1.5" gap, H_7, H_8, H_9, H_{10}, H_{11}
12. Stabilizer and rudder profiles in H_{12}, H_{13}, H_{14}, H_{15}, H_{16}, H_{17}
13. Stabilizer and rudder profiles in H_{18} and H_{19}
14. Vertical tail surfaces V_1, V_2, V_2', and V_4
15. " " " V_3, V_5, V_6, V_9
16. " " " V_7, V_8, V_{10}
17. Screen grid G to simulate slipstream effects on tail surfaces.
18. N.A.C.A. model 35 single float
19. Vertical cross-section through wind tunnel
20. Normal six-component rigging setup
21. Yaw-at-yaw rigging setup
22. Typical hinge-moment setup

Three-Component Measurements with Various Modifications

23. Effect of nacelles and of H_3V_3 with various stabilizer settings - three-component data
24. Effect of nacelles and of H_3V_3 with various stabilizer settings - parasite drag
25. Effect of H_2V_2v with various stabilizer settings, and effect of N - three-component data
26. Effect of H_2V_2v with various stabilizer settings, and effect of N - parasite drag
27. Effect of hull B_1, nacelles, and $H_{10}V_{11}$ with various stabilizer settings - three-component data
28. Effect of various components - parasite drag
29. Effect of various components with B_2 hull - three-component data
30. Effect of various components - parasite drag
31. Effect of flaps at various angles with and without tail surfaces H_2V_2v - three-component data
32. Pitching moment due to tail H_2V_2 with and without flaps
33. " " " " " H_3V_3 " " " "

INDEX OF FIGURES (cont'd)

Effects of Deflected Elevators; Elevator Hinge Moments

INDEX OF FIGURES (cont'd)

INDEX OF PHOTOS

1. WBN_cPH_3V, Run 6
2. " , " "
3. H_3V_6
4. H_2V_2, showing (left) bracket, b, on auxiliary fin
5. $WBPN_cH_2V_2V$, showing elevator hinge-moment rigging
6. " " " " "
7. $WBPH_cH_1V_2V$, showing setup for Run 96, elevators free, $e_t = -0.3e$
8. $WBPN_cH_{16}V_3G$, Run 261
9. $WBPH_cH_{16}V_3$, Run 280, showing setup for rudder hinge-moment tests with both rudders
10. Setup for Run 365, to determine tare hinge moment of rigging system used for twin rudders
11. WE_2P + fairing, Run 360
12. " " " " " "
13. Setup for Run 369: pitot tube in position to measure wake of rigging wire
14. " " " 370: " " " " " " " " " " "

TABLE 1

Notation Used to Describe Model Configurations

		Consol. Dwg. No.	Fig. No.	Photo No.
W =	wing (see Rep. 182)	29Z029	3	1, etc.
B =	hull of Rep. 182 (includes block for mounting tail surfaces	29Z020	4	"
B_1 =	B with revised hull bottom		4	
B_2 =	B_1 with revised forebody	29Z045	5	11,12
N_c =	Four nacelles with no airflow (Rep. 182)	29Z030	6	6
N_2 =	Four revised nacelles	29Z192	7	---
P =	Tip floats in retracted position at wing tips (see Rep. 182)	29Z029	1	6,9
H_1 =	original horizontal tail surfaces	29Z039	7	7
H_2 =	H_1 except elevator profile changed		8	4-6
H_3 =	horizontal tail surfaces for twin-tail arrangement	29Z040	9	1-3
H_{4-19} =	H_3 with successive changes of elevator profiles		9-13	8,9
H_{10}' =	H_{10} with wax removed between nose of stabilizer and hull		12	
V_1 =	original central (single) vertical surfaces plus outboard auxiliary fins (see note, Fig. 14)	29Z039	14	
V_2 =	V_1 except rudder profile changed (see note, Fig. 14)		14	4-7
V_3 =	twin vertical surfaces	29Z040	15	8,9
V_4 =	V_2 minus outboard auxiliary fins, but including brackets for fins		14	4
$V_{5,9}$ =	V_3 with changes of rudder profiles		15	
V_6 =	V_3 + central fin		15	3
V_7 =	V_6 with rudder size reduced		9,16	
V_8 =	V_3 with rudder size reduced		16	
V_{10} =	V_6 with piece of rudder removed at trailing edge		16	
V_{11} =	V_3 but with no hinge cutout and with correct center cutout		15	
V_2' =	same as V_2 except incorrect rudder nose length corrected (see note, Fig. 14)			

TABLE 1 (cont'd)

	Consol. Dwg. No.	Fig. No.	Photo No.
V_2'' = same as V_2' except unsymmetrical fin profile corrected (see note, Fig. 14)			
F_2 = hull fairing		4	
F = wing flaps; superscript indicates deflection in degrees		3	
V = gun turret (original)		4	
V_3 = " "		4a	
V_3^p = V_3 faired with wax behind			
V_4 = gun turret	29043	5	
W = waist gunner's turret	29019	5	
v = flow vanes at stern of hull			1,2,7
b = supporting brackets for outboard vertical surfaces of V_2			4
[illegible] = grid used to simulate slipstream effects		17	3
α_u = angle of attack relative to root chord line of wing, uncorrected for wind tunnel wall interference			
α = angle of attack relative to root chord line of wing, corrected for wind tunnel wall interference			
s = stabilizer angle relative to root wing chord line			
e = elevator angle relative to stabilizer			
e_1 = angle of center portion of elevators (over hull)			
e_t = elevator tab angle relative to elevator			
r = rudder angle relative to fin			
r_t = rudder tab angle relative to rudder			
ψ = angle of yaw relative to plane of symmetry			
i = angle of incidence of the wing relative to the deck line			
a_r, a_l = angles of right and left ailerons relative to wing chord			

TABLE 2

Dimensions full scale Model scale = 1:14

Main wing:

Root section = N.A.C.A. 23017.2, chord = 20 ft.

(Ideal) tip section = N.A.C.A. 23009, chord = 11 ft.

Mean aerodynamic chord (MAC) = t = 193.5 in.

	Wing + tip floats W	Horizontal Tail Surfaces $H_{1,2}$	Horizontal Tail Surfaces V_{8-10}, 12	Vertical Tail Surfaces $V_{1,2}$, V_2', V_2'' Main = V_4	Vertical Tail Surfaces $V_{1,2}$, V_2', V_2'' Aux.	Vertical Tail Surfaces $V_{3,5,9-11}$	Vertical Tail Surfaces $V_{6,7}$ Outboard	Vertical Tail Surfaces $V_{6,7}$ Central
Area, S, ft.^{2}	1750	209.27	330.10	97.17*	30.2 total of 2	130.12 total of 2	(see V_6)	63
Span, b, ft.	115	33.0	51.0	12.21*	5.0 each	10.71 each	"	(see Fig. 9)
Aspect Ratio, AR	7.43	4.04	7.46	1.54	0.0 each	1.27 each	"	"

*above horizontal tail

**dimensions are only nominal for V_{10} (see Fig. 16)

	Elevators $H_{1,2}$	Elevators H_{8-10}, 12	Elevators e_1	Rudders V_2', V_2''	Rudders $V_{3,5,9,11}$	Rudders $V_{7,8,10}$*	Ailerons, a
S_{aft}, area aft of hinge line, ft.^{2}	103.2	87.95	14.50	54.61	77.72 total of 2	59.90 total of 2	60 each
t_{aft}, mean chord of S_{aft}, ft.	3.65	3.0	2.12	4.0	3.47 each	2.70 each	3.34
Tab area, ft.^{2}	6.02	5.4	0	5.47	4.52 total of 2	4.52 total of 2	---

*dimensions are only nominal for V_{10} (see Fig. 16)

Note: Wing area includes portion covered by hull and area of tip floats (the latter = 50 sq.ft.)

Horizontal tail areas include portion covered by hull.

Tail length = { [illegible] to elevator hinge line = 40.42 ft. / [illegible] to rudder hinge line = 41.58 ft.

REPORT ON
ADDITIONAL WIND TUNNEL TESTS ON A 1/14th SCALE MODEL OF THE CONSOLIDATED XPB2Y-1 FLYING BOAT, WITH PARTICULAR REGARD TO TAIL SURFACES

I. Introduction, General Description of Model and Tests

This Report describes the results of wind tunnel tests on a 1/14th scale model of the Consolidated XPB2Y-1 Flying Boat. These tests were supplementary to those discussed in CALCIT (Guggenheim Aeronautics Laboratory at the California Institute of Technology) Reports 170, 170-A, 170-B, and 182. The experiments were made in the closed working section of the 10-foot wind tunnel of the GALCIT.* All of the tests were made at a wind speed of about 175 m.p.h., corresponding to a Reynolds Number based on mean wing chord of approximately 1,600,000. The critical Reynolds Number at which a 15 cm. sphere has a drag coefficient of 0.3 is about 325,000, indicating a wind stream with very low turbulence. The entire model was lacquered and rubbed down to a high polish.

During the course of the investigation, many modifications were made. Table 1 (page 19) gives the notation employed throughout the Report in designating the various elements and configurations. Several of the component parts of the model are shown in Figs. 1-18. A three-view of the airplane with full-scale dimensions is given in Fig. 1. On this figure are indicated the C.G. location and the mean aerodynamic chord (M.A.C) dimensions and locations which were used in reducing the experimental data. The full-scale data which were

---

*cf. Clark B. Millikan and A. L. Klein: "Description and Calibration of 10-Foot Wind Tunnel at California Institute of Technology", presented at the Berkeley meeting, Aeronautics Section of the A.S.M.E., June 1932.

furnished by the Consolidated Corporation and used throughout the report are given in Table 2. For details of the model and its parts reference must be made to the original Consolidated Corporation drawings (cf. Table 1).

The tests were divided into the following broad groups:

1) Three-component measurements with various modifications
2) Effects of deflected elevators; elevator hinge moments
3) Yawing moments at angles of yaw for various configurations
4) Effects of deflected rudders; rudder hinge moments
5) Aileron hinge moments

The results will be discussed in terms of the above grouping in Section III.

II. Method of Making Tests and Calculations, and of Presenting Results; Notation

The normal experimental setup is indicated schematically in Figs. 19 and 20, and is illustrated by the Photos at the end of the Report. The tare drag and moment of the supporting system were estimated from the experimental results of previous GALCIT investigations. The tare drag at the high-speed attitude of the airplane was approximately 40% of the total net parasite drag at small angles of attack. A special setup for yawing moment at angles of yaw is illustrated in Fig. 21 and described in Section III,3 below. A typical setup for investigating hinge moments is illustrated in Fig. 22 and discussed in Section III,2 and 4.

All drags, angles of attack, and pitching moments were corrected by the Millikan and Lotz theories of tunnel wall interference* to give free air conditions. Yawing and hinge moments were not corrected for tunnel wall interference.

---

*Millikan, C. B.: "On the Lift Distribution for Wings of Arbitrary Plan Form in a Circular Wind Tunnel"; Proc. A.S.M.E., App. Mech., Sept. 1932.

Lotz, Irmgard: "Korrektur des Abwindes in Windkanälen mit kreisrunden oder elliptischen Querschnitten"; Luftfahrtforschung Vol. 12, No. 8 (1935).

All observations were reduced to the standard American system of absolute units.

$C_L = \frac{\text{lift}}{qS}$ $C_D = \frac{\text{drag}}{qS}$ $C_m = \frac{\text{Pitching Moment}}{qSt}$

$C_y = \frac{\text{Yawing moment}}{qSb}$ $C_l = \frac{\text{rolling moment}}{\text{(lift on } S_{aft}\text{)} \, t_{aft}}$

where

q = dynamic pressure = $\frac{\rho}{2} V^2$ ($\frac{\text{lb.}}{\text{ft.}^2}$)

ρ = mass density of air (note: a correction was applied to the experimental observations so that in this formula ρ is to be taken as the free air density uncorrected for compressibility effects, at least up to 200 m.p.h.)

V = velocity

S = wing area including area of tip floats in flying position (see Table 2)

t = aerodynamic chord (see Table 2)

b = span (see Table 2)

S_{aft} = area of movable control surface aft of hinge line (cf. Table 2)

t_{aft} = mean chord of movable control surface aft of hinge line (cf. Table 2)

The coordinate axes are the same as those used by the N.A.C.A. C_m is positive when it tends to raise the nose; C_y is positive when it tends to move the nose back, and the angle of yaw, ψ, is positive when the nose is yawed to the right. Control surface angles are positive when they increase the lift (or side force to the right) on the surface. Hinge moments are positive when they tend to decrease the angle of the movable surface in question.

In certain cases the parasite drag coefficient C_{D_p} was determined, the formula employed being:

$$C_{D_p} = C_D - \frac{C_L^2}{\pi AR}$$

where AR = aspect ratio = $\frac{(\text{span})^2}{\text{area}}$. It will be noticed that the lift distribution was assumed to be elliptical.

All pitching-moment coefficients are referred to the ... position, ... i. l. The scale of ... is referred to the root chord line at all times.

It should be mentioned that the plotted experimental points represent direct observations with no fairing, except that the tare drag and moment results were faired before being subtracted from the observed total drags and moments to ... [illegible]. All re- ... [illegible] ... [illegible].

... [illegible]

1 ... [illegible] ... [illegible]

... [illegible] ... presented three-component data showing the effects of nacelles n_c and twin tail surfaces n_g/g. The customary nacelle effects appear; i.e., increase of drag, decrease of longitudinal ... [illegible], and decrease of maximum lift. Addition of tail ... [illegible] ... approximately $(-d\sigma_l/d\alpha_l) = 0.10$ for ... [illegible] ... The ... [illegible] ... is approximately $(-d\sigma_l/d\alpha_l) = -.2$ ... [illegible]. The experimental parasite drag curves are shown in ... [illegible]. The ... [illegible] ... [illegible].

... [illegible] ... tail surface configuration "g/g" (large central vertical tail plus auxiliary outboard fins plus vanes on rear of hull) and of the original gun turrets. This tail arrangement reduces ... [illegible] ... $(-d\sigma_l/d\sigma_l) = .11$ for $\alpha = -1^\circ$ and ... for $\alpha = 1.7^\circ$. The ... [illegible] ... is about 0.024 per degree. The airplane characteristics are not greatly affected by the gun turret, except that a considerable

change in C_L for trim with elevators neutral occurs. The corresponding parasite drag effects are presented in Fig. 26. The increments are again given in Table 3, below.

In Fig. 27 are shown the characteristics of various configurations with hull H_1; i.e., with revised hull bottom lines (cf. Fig. 4). The effects of the various components are those usually observed. The complete model has a static stability of about $(-dC_y/dC_L) = 0.19$.

The corresponding parasite drag results are included in Fig. 28. The drags of H_1, N_c, and $N_{18}V_{11}$ are included in Table 3, below. The drag of the gun turret T_3 (cf. Fig. 4a) is seen to amount to $\Delta C_{D_T} = 0.0009$, practically independent of C_L. This increment is decreased nearly 50% by wax fairing behind the turret.

Run 337, with the large single float attached to the wing, was made in order to determine the drag of the N.A.C.A.-35 type of float (cf. Fig. 12), and has no particular reference to the XPY-1 airplane.

The results of Runs with the revised hull, H_2, are presented in Figs. 29 and 30. The effects of turrets, nacelles, and tail surfaces are similar to those discussed above for analogous configurations. The static stability of the complete model is $(-dC_y/dC_L) = 0.19$. In Fig. 30 a comparison of Runs 359 and 360 discloses that the wax hull fairing shown in Photos 11 and 12 caused an increase of drag. This should not be considered as conclusive evidence that the revised hull lines are worse than the original ones, since similar effects have often been observed at the GALCIT when fuselage or hull contours have been modified by wax fairing. It is therefore believed that the increased roughness of the wax surface may be sufficient to account for the

increment of drag. The drags of both turrets, T_3 and T_4, are very small. The increments due to nacelles and tail surfaces are discussed in connection with Table 3, below.

Table 3, which follows, shows the parasite drag coefficients of various major elements based on wing area, and also the "proper drag coefficients" of some based on projected area. For nacelles and hulls the latter is the total frontal area including any wing area covered by the element. It was given by the Consolidated Corporation. For tail surfaces, the total tail area of Table 2 was taken. For nacelles and hulls, C_{D_p} was determined at $C_L = 0.50$ corresponding to an assumed cruising condition. For tail surfaces, the C_L of zero tail load was taken as the abscissa for determining C_{D_p}.

TABLE 3

[illegible] areas

Element	[illegible] drag increment, ΔC_{D_p} (based on wing area, 1760 ft.^{2})	C_L	Fig. for ref.	"Proper" area of element S_p, ft.^{2}	"Proper drag coeff.", $C_{D_p} = 1760\ \Delta C_{D_p}/S_p$
Nacelles, N_c	0.0032	.5	24	12.[illegible] x 4	0.111
Nacelles, [illegible]$_c$	[illegible]	"	[illegible]	"	0.118
Nacelles, [illegible]$_2$	[illegible]	[illegible]	[illegible]	21.[illegible] x 4	0.066
Tail Surfaces, [illegible], $\delta = -1^\circ$	0.0027	[illegible] (cf. Fig. 25)	24	507.12	0.0095
Tail Surfaces, [illegible], $\delta = -1^\circ$	0.0047	[illegible] (cf. Fig. 25)	26	516.04 (not incl. v)	0.0158
Tail Surfaces, [illegible], $\delta = -1^\circ$	[illegible]	[illegible] (cf. Fig. 27)	28	306.12	0.0109
Tail Surfaces, [illegible], $\delta = -1^\circ$	0.0030	[illegible] (cf. Fig. 27)	30	"	0.0106
Hull, [illegible]	[illegible]	[illegible]	28	113	0.102
Hull, [illegible]	[illegible]	"	24,28	"	[illegible].112
Hull, [illegible]$_2$	[illegible]	"	28,30	130	0.100

The most interesting results in Table 3 are the extremely small value of the coefficient C_{D_π} for nacelles [illegible]$_2$ and the large value for [illegible].

The effects of wing flaps at various angles with various configurations are shown in Fig. 31.

From the tail-on and tail-off Runs of Figs. 23 and 31, several curves of pitching-moment coefficient due to tail surfaces have been obtained by subtraction. These are plotted in Figs. 32 and 33. From

[illegible] [illegible]

[illegible] [illegible]

[illegible] tail efficiency factor, η_t, [illegible] [illegible] [illegible]. From the data given [illegible] Table 2 [illegible] [illegible] for the slope [illegible]:

$$(-dC_m/d\delta_e)_{t,\,cor.} = 0.237\ \eta_t \text{ for } [illegible]_2 [illegible]_2$$

$$= [illegible]\ \eta_t \text{ for } [illegible]_3 [illegible]_3$$

The experimental slopes measured [illegible] [illegible], and the corresponding values of the tail efficiency factor, are as follows:

		$(-dC_m/d\delta_e)$	η_t
[illegible]	[illegible]	[illegible]	[illegible]
	[illegible]	[illegible]	[illegible]
[illegible]	[illegible]	[illegible]	[illegible]
	[illegible]	[illegible]	[illegible]

These values of η_t are approximately the same as those usually obtained at the [illegible] GALCIT for flying boats with single and twin vertical tail arrangements, respectively. The increase in η_t with flaps deflected over that with flaps up, which occurs for $[illegible]_2 [illegible]_2$, is unusual.

[illegible]) [illegible] [illegible] [illegible]
([illegible])

The data of this section cover primarily the effects on hinge moment and [illegible] of small [illegible] [illegible] to the elevators. The first ten figures give the results of tests on the single-tail arrangement (i.e., $[illegible]_1$ and $[illegible]_2$), while the remaining thirty-seven figures are concerned with modifications to the twin-tail arrangement, be-

---

* [illegible], [illegible]: "Effect of Slipstream on the Longitudinal Stability of [illegible] Monoplane"; Jour. Aero. Sci., Vol. 4, No. 10, August [illegible].

ginning with R_3. The hinge-moment data were obtained by the customary GALCIT procedure illustrated in Fig. 22. In this method, hinge moments are applied to the movable surface by means of a fine piano wire attached to the trailing edge. The angle assumed by the surface under the influence of this hinge moment is then observed visually on a protractor scale fastened to the model. Before making any such Run, a careful check was made to insure that the friction in the hinges was small enough to be negligible. All hinge moments have been corrected for any "static" hinge moment which appeared (i.e., any measuralle unbalance of the system with the tunnel airstream off), but no attempt has been made to correct the hinge moments for aerodynamic tare moments of the piano-wire rigging system.

One new element of technique was introduced in the present tests. Simultaneously with many of the hinge-moment Runs, readings were taken on the normal three- or six-component balances to determine the characteristics of the model with various elevator deflections. In the computation of these data, the lift and pitching moment introduced by the hinge-moment weights hanging from the model have been subtracted from the respective measured values. However, no correction has been made for the additional tare drag or tare moment caused by the piano wires. The results of these Runs have, in most cases, been plotted as in Fig. 23; i.e., $C_{m_{c/4}}$ and $C_{h_{\delta_e}}$ as functions of α for various angles of attack, and, below, α vs. C_L and cross-plots of $C_{h_{\delta_e}}$ vs. C_L. Included in many of the Figures are drawings showing the established elevator profiles of the configuration in question.

The hinge-moment and pitching-moment data for several of the configurations were supplemented by elevator-free stability Runs; i.e., Runs in which the lift, drag, and pitching moment were determined

as functions of the angle of attack in the normal manner but with the elevators free to rotate on their hinges. In these tests the elevator hinge-moment rings were removed from the model, and sufficient weight was applied through them to counteract the static unbalance of the elevators. The pitching moment and lift were corrected for this tare weight, but not for the presence of the wires. The angles assumed by the elevators under the various conditions were observed and recorded. The values of these angles observed during elevator-free tests were in poor agreement with the angles for $C_{h_e} = 0$ for the same configuration and angle of attack as determined from the hinge-moment curves. This occurs in all the elevator-free runs in Figs. 35-42, i.e., for the horizontal surfaces H_1 or H_2. Hence it appears that there was excessive friction or other unsatisfactory bearing conditions in these units. These conditions were apparently remedied in the revised tails (H_{3-10}), for good agreement was found between all subsequent elevator-free and hinge-moment runs with the exception of two cases which are discussed below (Figs. 51 and 67).

The general procedure in these tests consisted of careful study of the data [illegible] and subsequent tail [illegible] of the tail arrangements [illegible] of the results thus obtained. In view of this [illegible] the experimental results in this section will be confined primarily to the most satisfactory tail configurations.

The data presented in Figs. 34-43 give certain characteristics of the original horizontal surface H_1 and of H_2, which differed only in the profile of the elevator-balance nose, as sketched. The average slope of the hinge-moment curves for H_1 with Flettner tab (Fig. 34) is

[illegible] C_{m_α} [illegible] early uniform over a range of $\pm 5^\circ$ or $\pm 6^\circ$ of elevator deflections. Comparison of [illegible] to a more [illegible] (δ_e) is [illegible] ($d\delta_e/dC_L$). The use of the linkage ($\delta_t = -0.7\delta_e$) also decreases the stiffness of C_{m_1}, but the curves remained (Fig. 34) are not constant in slope. It is seen that a small stable [illegible] with elevators free with this tab linkage in use (Run 99). Considerable unstable instability occurs, however, with the linkages of Runs 1 [illegible]; i.e., with the linkages arranged so that the tab is at 5.5° or 6° relative to the elevator when the elevator angle is 0°. The appearance of non-linearities in the variation of C_{m_α} with angle of attack ($dC_{m_\alpha}/d\alpha_w$) with T_2 (Fig. 36) in Runs 79-81 led to repetition of Run 80 in Run 113 [illegible] of Runs 113 and 117, as indicated. The agreement between the two sets of Runs is fairly good in regard to the slopes $d\alpha_w/d\alpha$ and $d\alpha_w/d\alpha_t$, but the magnitudes of C_{m_α} do not agree. Since the tail assembly was removed from the model between the two sets of Runs, the discrepancy may have been caused by errors in reproduction [illegible]. The effect of stabilizer setting is [illegible]. (T. [illegible] stability constants ($C_{m_{T_2}}$) available from elevator deflections with T_2 (Fig. 35) are small [illegible] to Table [illegible] values.

[illegible] Fig. 38 were intended to simulate, as best as practical, the effect of slipstream on the tail. The [illegible] over the central portion of the tail by a screen, 6 (cf. Fig. 17 and Photo 2). This had the effect of weighting [illegible] outboard portions in a manner analogous to the slipstream effect in flight. Although the aerodynamic balance area of the sections outboard was relatively greater than inboard, no indications of overbalance appear in Fig. 38.

[illegible]

[illegible] coefficients plotted have been based upon the free-stream value of q, the dynamic pressure. Hence the [illegible] limits of the slope dC_m/dc_t is not a measure of the slipstream effect, and only its sign is of any interest.

Figs. 39-41 give the effects of wing flaps and elevator [illegible] on the lift moments of T_2. Figs. 42 and 43 show that a small elevator-free stability is obtained with a 10° tab deflection, [illegible] assumed.

Figs. 44-46 are from [illegible] drag data concerning the effects of deflected elevator with T_2, flaps up and down. The pitching moments produced by large elevator deflections are relatively small. The maximum stalling [illegible] obtained [illegible] some advance [illegible].

Figs. 47-50 show the [illegible] of the [illegible] configurations. [illegible] tail assembly [illegible] the [illegible] of C_{m_0} [illegible] $1.0°$-$1.5°$. [illegible] $|\epsilon| > 1.5°$ or $12°$, [illegible] extremely large. In addition [illegible], particularly [illegible] small [illegible]. [illegible] elevator-free stability [illegible] practically unacceptable, [illegible] bear little relation to the values for $C_{m_0} = 0$ in Fig. 50. It seems probable that the [illegible] changes of elevator deflection which appear were caused by [illegible]. [illegible] small [illegible] and [illegible] range $1.5° > \epsilon > -2°$. The elevator-free stability with flaps (Fig. 42) is [illegible].

In Runs 100 and 101, with H_4V_3, (cf. Fig. 10) it was found that the square elevator nose produced violent overbalance, and the Runs were not completed. No readings were made of the hinge moments or pitching moments.

Figs. 53-56 show the results of a progressive series of modifications to the elevator nose of H_4. In H_5 the sharp corners were slightly and symmetrically rounded, in H_6 the lower corner only was further rounded, and in H_7 the upper corner was rounded to match. The corresponding hinge-moment curves show a consistent increase of stiffness for small deflections, together with a decrease in stiffness for large deflections; i.e., a consistent tendency for the C_{h_e} curves to become straighter.

In Figs. 57-62 are shown the elevator characteristics with H_8, which differs from H_7 only in the width of elevator-stabilizer gap (cf. Fig. 10). In Figs. 57 and 58 it is seen that the hinge-moment curves of H_8 are practically uniform in slope over a 40° range of deflections. The mean slope for this range is approximately $dC_{h_e}/de = 0.006$ per degree. The slope $dC_{h_e}/d\sigma_u$ also appears to be nearly uniform. The stalling moments produced by elevator deflections are larger than in any of the configurations discussed above. In Fig. 59 it is seen that rudder deflection does not appreciably affect the elevator hinge moment. Figs. 60 and 61 show the elevator tab effectiveness at two angles of attack. Also in Fig. 60 it is seen that an elevator-free stability of $(-dC_m/dC_L) = 0.15$ is obtained. This is nearly 80% of the elevator-fixed stability (cf. Fig. 23). The effects of 2:1 and 3:1 tab linkages are shown in Fig. 62. Either linkage has the effect of reducing dC_{h_e}/de to about 0.005 per degree, and an elevator-free stability of 0.14 is maintained.

Fig. 63 consists of a collection of elevator-free stability data for the twin tails discussed above. The superiority of H_8 is apparent.

In H_9 (Figs. 64-66) the aerodynamic balance area was increased as indicated. The characteristics of the elevator are similar to those of H_8, except that the mean control stiffness is decreased to slightly over 0.005. The percentage of balance area was again increased in H_{10} (Fig. 67), but at the expense of uniformity in both dC_{H_e}/de and $dC_{H_e}/d\alpha_u$. The elevator-free stability test with H_{10} (Run 207, Fig. 67) was apparently made with excessive friction or interference between parts, which caused the elevator angle to vary erratically, as shown. A slight improvement in this regard, at least for negative elevator deflections, was obtained in H_{11} (Fig. 68), in which the lower part of the balance portion was cut away slightly. Elevator-free stability curves for $H_{8,9,11}$ are plotted in Fig. 69, where it appears that the elevator-nose modifications had little effect.

In Fig. 70 are shown the hinge-moment characteristics of H_{12}, which was the same as H_{11} except that the aerodynamic balance portion was made slightly thicker in profile. A slope $dC_{H_e}/de = 0.004$ per degree was obtained for small deflections, but the curves are not straight and the undesirable crossing of the curves for various α_u's remains.

Figs. 71 and 72 give the results of several unsuccessful modifications to the elevators. These changes, which are explained by sketches and notes on the Figures, all produced rather undesirable hinge-moment curves.

H_{16} (Figs. 73-76) had a slightly unsymmetrical balance profile, as indicated. Its characteristics include an average stiffness of about 0.005 per degree, nearly uniform over a 24°-26° range of deflections, and a uniform elevator-free stability of 0.14 (flaps up). There is a tendency for the C_{H_e} curves for various α_u's to run together at small positive values of e, but no definite indications of crossing appear. The stalling moments due to elevator deflections are large. The attempt to simulate conditions with slipstream was repeated with this configuration (Fig. 75), and again no overbalance resulted.

Figs. 77-80 give the elevator characteristics of H_{18} and H_{19}, which were equipped with elevators with asymmetrical balance profiles which varied along the span, as indicated in the sketches. Of these two configurations, H_{19} had slightly greater aerodynamic balance area and its balance noses were sharper in profile. The hinge-moment curves for H_{18} have about the same slope (dC_{H_e}/de) for small deflections as those of H_9 or H_{16}, above, but the slope is uniform over a range of only 20°-22°. In the case of H_{19} the slope is somewhat less, but the range of constant slope is still less. One extremely undesirable effect appears in Figs. 77-80; i.e., a serious decrease in the maximum stalling moment available from elevator deflections.

3) Yawing Moments at Angles of Yaw for Various Configurations (Figs. 81-85)

Fig. 81 shows the directional stabilities of various configurations in which the components of the tail arrangement H_2V_2v were progressively added to the model. The effect of the hull fairing F_2 (cf. Fig. 4) on the model minus tail is also shown, and it is seen that this modification increased the instability of the hull at large angles

of yaw. Addition of the horizontal tail, H_2, with the brackets, b, for the auxiliary fins reduced the instability at large angles, but subsequent addition of the tail vanes, v (cf. Photos 5-7), on the stern of the hull had little effect. A curious, asymmetrical discontinuity appears in the curve for Run 9 between $\psi = 3^\circ$ and $\psi = 6^\circ$. Indications of the same effect are seen in Run 10. The central vertical tail surfaces, when added to this configuration to form H_2V_4v, produced an average directional stability of $(-dC_y/d\psi) = 0.0007$ per degree (for $-15^\circ < \psi < 15^\circ$). A pronounced loss of stability occurs in the curve for this configuration (Run 8) near $\psi = 0^\circ$. Moreover, the asymmetrical behavior near $\psi = 3^\circ$ noted above appears again. The yawing moment due to the vertical surface (Run 8 minus Run 9) is very nearly a linear function of ψ. The addition of the auxiliary fins to H_2V_4v forms the complete empennage, H_2V_2v, which has a stability of 0.0010 per degree (average for $-15^\circ < \psi < 15^\circ$. This is somewhat less than usually recommended for flying boats.

In Fig. 82 it is seen that the addition of H_3 (which has considerable dihedral angle, cf. Figs. 1 and 9) to the model minus tail decreases the instability greatly, especially at large angles of yaw. Again the vanes v have only a minor effect. Addition of the vertical surfaces produces a stability of 0.0013 per degree (average). The indicated slope near zero yaw is considerably less (about 0.0005 per degree). Again this is an effect carried over from the characteristics of the model minus tail, for the yawing moment due to V_3 is nearly linear in ψ.

The effects of changes of nacelles and hull are seen in Fig. 83. The increased instability with the large nacelles, N_2, is noteworthy. B_1 is also slightly more unstable than B, as would be

expected (cf. Fig. 4). The complete configuration (Run 372) has a stability (average) of about 0.0013 per degree, which is not affected by addition of gun turret M_3. Fig. 84 shows the effect of $H_{18}V_{11}$ on the model with B_2 and N_2. The average stability produced is about 0.0012 per degree, and again the addition of turrets has no appreciable effect.

The tests reported in Fig. 85 were conducted in an effort to determine the interference effects of the yaw-at-yaw rigging system on the vertical tail surface. A pitot tube was attached to the model in three different positions near the vertical tail location, as shown in Fig. 85 and Photos 13 and 14. The angle of yaw of the model was then varied in the usual manner and the variation of the dynamic pressure at the tube was determined. The results are plotted in Fig. 85 for the three pitot-tube locations. It is apparent that a wake was encountered behind the rigging strut (i.e., at $\psi = 0^\circ$ for Positions 1 and 2) and behind the rigging wire ($\psi \doteq -6^\circ$, Position 3). In both of these wakes the dynamic pressure was 12%-15% lower than outside. The conclusion to be drawn is that tests made in the present GALCIT yaw-at-yaw rigging system may indicate irregular results in cases where any vertical tail surface lies behind a rigging wire or strut.

It is important to reconsider the data of Figs. 81-84 in the light of these results. Since the yawing moment due to vertical tail surfaces is nearly linear in ψ for both Run 2 and Run 8 in Fig. 81, it appears that no appreciable strut-wake effect occurred. However, the curves of Runs 1, 372, 373, 366, and 367, in Figs. 82-84, show slight decreases in yawing moment due to tail at $\psi = \pm 6^\circ$, as compared to smooth curves faired through the other experimental points. It is possible that this is the effect of the rigging-wire-wake on the outboard vertical surfaces. The effect is not great enough to alter the conclusions of the preceding paragraphs.

4) Effects of Deflected Rudders; Rudder Hinge Moments (Figs. 86-106)

The rudder hinge-moment data presented in this section were obtained by the usual GALCIT hinge-moment method as described in Section III,2 above. In many Runs the yawing moment balance was read simultaneously, and the procedure in computing and presenting the results was analogous to that described in detail above. The results discussed at the end of the preceding section indicate that all data obtained with a central vertical tail surface at $\psi = 0^\circ$ or with the twin vertical surface arrangements at $\psi = \pm 5^\circ$ are to be considered somewhat unreliable.

Figs. 86-88 are concerned with the characteristics of V_1, V_2, and V_2', which were all discovered to be of faulty construction, as noted in the Figures. Fig. 89 shows that V_2'', which was accurately made, had an average rudder-control stiffness of $dC_{H_r}/dr = 0.004$ per degree, but that this slope was not uniform and that overbalance occurred for all but two angles of yaw. The maximum yawing moment obtained ($C_y = 0.0235$) is rather small. The variation of hinge moment with yaw angle ($dC_{H_r}/d\psi$) is not uniform. The rudder-free directional stability curve is difficult to interpret, and probably indicates friction in the rudder system.

Figs. 90 and 91 show the characteristics of the rudder in V_3 with horizontal tail H_3 in use. Fig. 92 gives the same data for V_3 with H_{16}; hence the two sets of data should show the same results, since H_3 and H_{16} differ only in elevator-nose profiles. However, the hinge-moment data of Fig. 90 were obtained with only one rudder in place, while those of Fig. 92 were obtained with both rudders attached together. Comparison of the two sets of curves discloses fairly good agreement for negative values of r, but poor agreement for positive

values. In view of the asymmetries of the curves of Fig. 90, it seems probable that they are the less reliable of the two sets. Fig. 92 shows a mean stiffness of $dC_{H_r}/dr = 0.005$ per degree near the symmetrical condition, approximately uniform stiffness for about 20° of rudder deflection, uniform $dC_{H_r}/d\psi$, large yawing moments available from full deflections ($C_y \doteq 0.036$ at $\psi = -15^\circ$ and $r = -24^\circ$). Figs. 93 and 94 give the rudder tab effectiveness with V_3. In Fig. 95 it is seen that a 2:3 tab linkage reduces the stiffness slightly, but also causes some crossing of the curves. A 1:1 linkage reduced the stiffness still further but produced overbalance at angles of yaw different from zero (no data were recorded). In Fig. 96 it is difficult to recognize any consistent and definite effects on the directional stability.

Fig. 97 is a compilation of directional-stability curves for various single, twin, and triple vertical tail arrangements. The rudder-fixed stabilities have been discussed above, with the exception of that produced by V_6, where $V_6 = V_3$ + a central vertical surface. It is seen that the central surface increases the stability by about 0.0003 per degree. The rudder-free stability curves are again difficult to interpret, but it appears that the stability is somewhat greater with V_2 than with V_3.

In Figs. 98 and 99 are shown the characteristics of two rudders which differ from those in V_3 only in the profiles of their aerodynamic balance portions. The data of Fig. 98 were taken on the right rudder only, and exhibit the same type of asymmetry as noted above in connection with Fig. 90. The sharp projecting corners in V_5 produce a small control stiffness for small rudder deflections, but this is maintained over only a small range. The rudders in V_9

have about the same stiffness as those in V_3 (cf. Fig. 92) for small deflections, but they are less stiff for large deflections; i.e., maximum rudder deflection may be reached with less control force. The maximum yawing moment coefficient produced at $\psi = -15^\circ$ is 0.038 at $r = -25^\circ$. This is greater than for V_3.

V_{11}, the characteristics of which appear in Figs. 100 and 101, was the same as V_3 except that the rudder hinge cutouts of V_3 (i.e., the portions of the rudder balance cut away to provide passage for the hinge supports) were corrected to agree more closely with the twin tail arrangement which was used in flight tests of the XPB2Y-1 airplane by the Consolidated Corporation. Comparison of Figs. 92 and 100 discloses that the small additional aerodynamic balance area did not appreciably affect the control stiffness near $r = 0^\circ$, and that the stiffness for extreme deflections was slightly increased by the change. From Figs. 94 and 101 it appears that the tab effectiveness was not appreciably affected.

Fig. 102 gives the characteristics of the outboard rudders in V_7, which was the same as V_6, except that the rudder hinge lines were moved aft and the rudder area decreased (cf. Fig. 16). The hinge-moment curves (based on the new area and mean chord) show an average slope for small deflections of $dC_{H_r}/dr \doteq 0.007$ per degree. They are roughly uniform in slope over a range of about 25°. There is some indication of non-uniformity in $dC_{H_r}/d\psi$. The yawing moments produced by rudder deflections are very great ($C_y \doteq 0.042$ at $\psi = -15^\circ$ and $r \doteq -24^\circ$). The rudder-free directional stability is large and reasonably uniform.

Fig. 103 shows the rudder-free directional stabilities of various configurations. The stability with V_8 (i.e., V_7 minus central fin) with tabs neutral is about the same as that with V_6 (i.e., V_3 + central fin) with a 2:3 tab linkage. The stability with V_7 is considerably greater, due to the effect of the additional vertical tail area.

V_{10} was formed by trimming off part of the rudder area of V_8, as indicated in Fig. 16. Its characteristics are shown in Fig. 104, where the hinge-moment coefficients are based on the "nominal" area and chord (same as V_8) rather than on the actual values. This enables one to obtain a comparison of the stick forces with V_8 and V_{10} directly from the C_{H_r} curves. From a comparison of Figs. 104 and 102 (note that the rudders of V_7 and V_8 are identical) it appears that the control stiffness has been decreased to $dC_{H_r}/dr \doteq 0.005$ per degree (average for small deflections) and that the yawing moments obtained from rudder deflections have been considerably decreased. The maximum yawing moment obtained is 0.032. The rudder-free stability was also decreased by the change.

The curves of Figs. 105 and 106 are the results of a brief investigation of the tare hinge moments produced by the struts which were used to connect the rudders in the twin-tail configurations (i.e., in $V_{3,5-11}$). The struts are pictured in Photo 9, where it is also seen that a small "sting" or bracket projected from the trailing edge of each rudder in these tests. Fig. 105 shows the results of replacing the strut by a piano wire. The slope dC_{H_r}/dr was reduced about 0.001 per degree (for small deflections) by the change, and C_y curves were not appreciably altered, and the rudder-free stability seems to have been increased slightly. Use of the wire connection

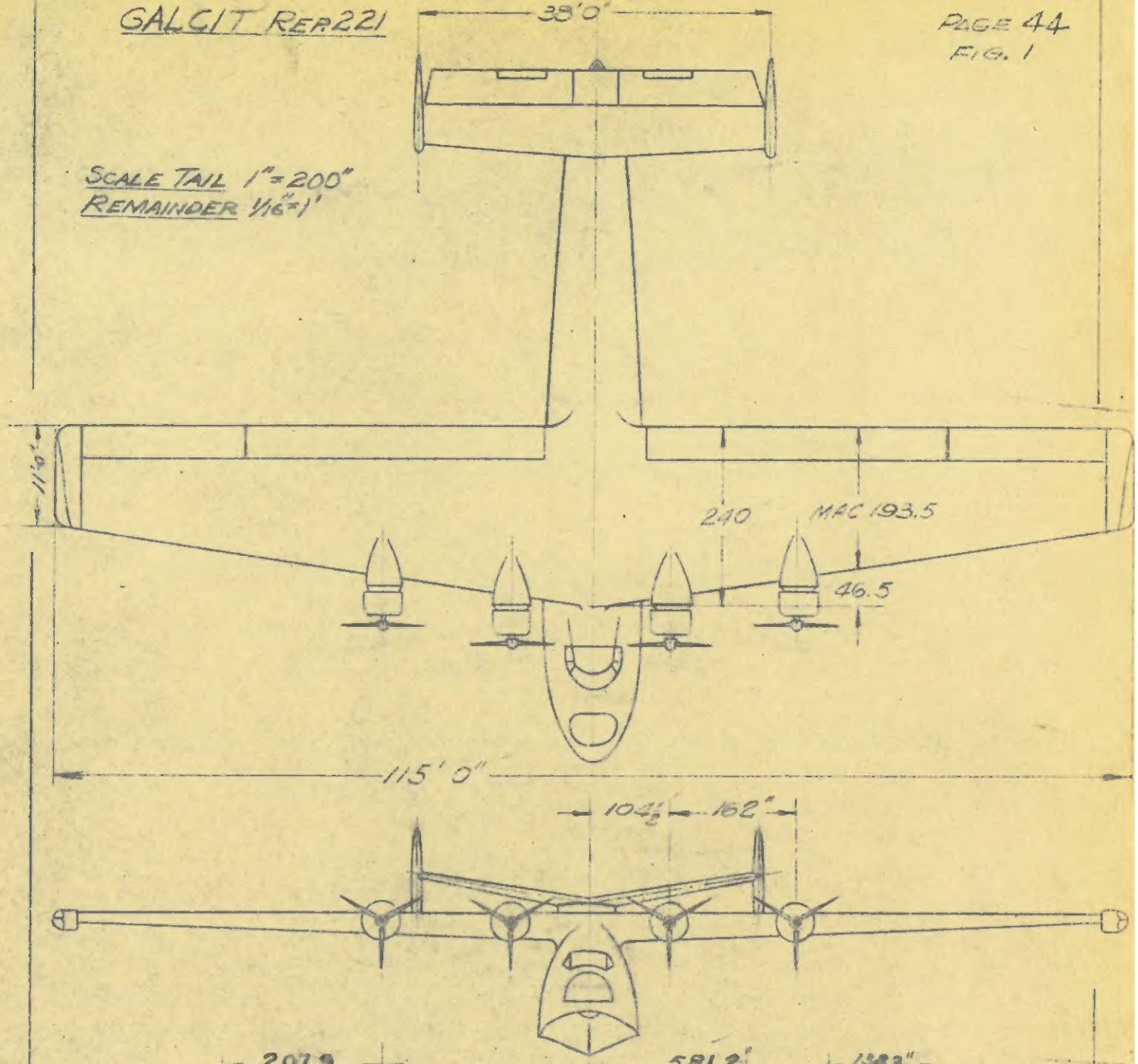

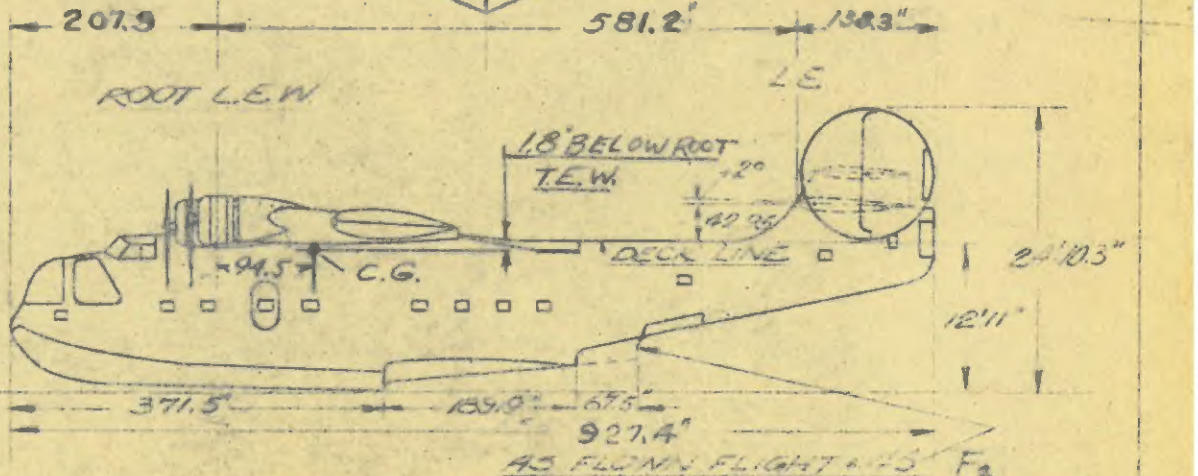

REF. DRAWINGS
M-1061 OF 8-12-37
AND 29E190 OF 8-9-38

INCIDENCE OF WING +3° TO THE DECK LINE
℄ T. PARALLEL TO DECK & LONGITUDINAL
AXIS. ROOT CHORD LINE REF. FOR <

CONSOLIDATED AIRCRAFT CORP.
XPB2Y-1

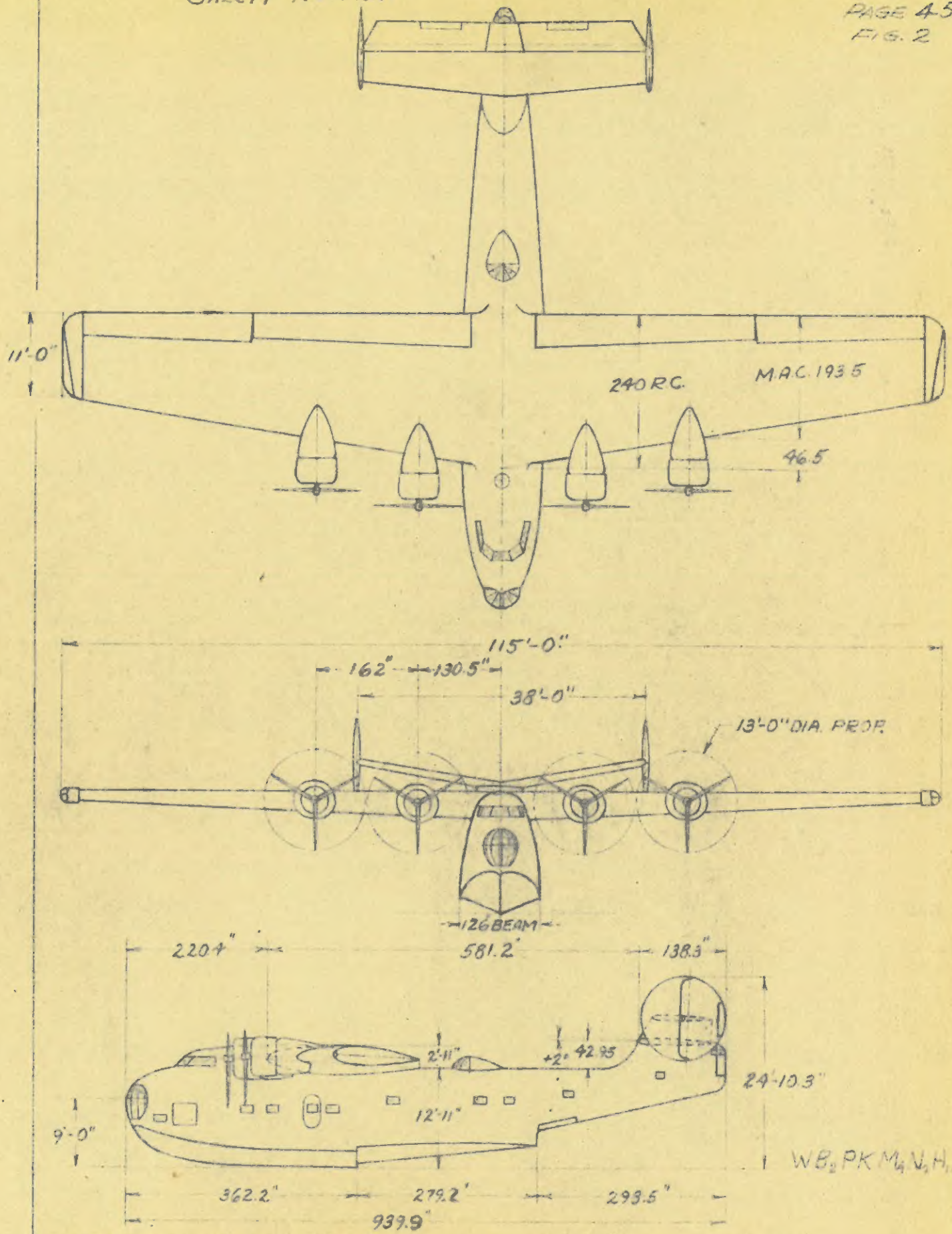

INCIDENCE OF WING +3° TO DECK LINE
℄ OF THRUST PARALLEL TO DECK & LONGITUDINAL AXIS. ROOT CHORD REF. FOR ∝.
SAME C.G. LOCATION AS PREVIOUSLY USED.

XPB2Y-1 CK. JOH
PROPOSED PRODUCTION MODEL
REF. DWG. 29R274 SCALE 1"=200"

CONSOLIDATED AIRCRAFT CORPORATION

MODEL AIRPLANE REPORT NO.

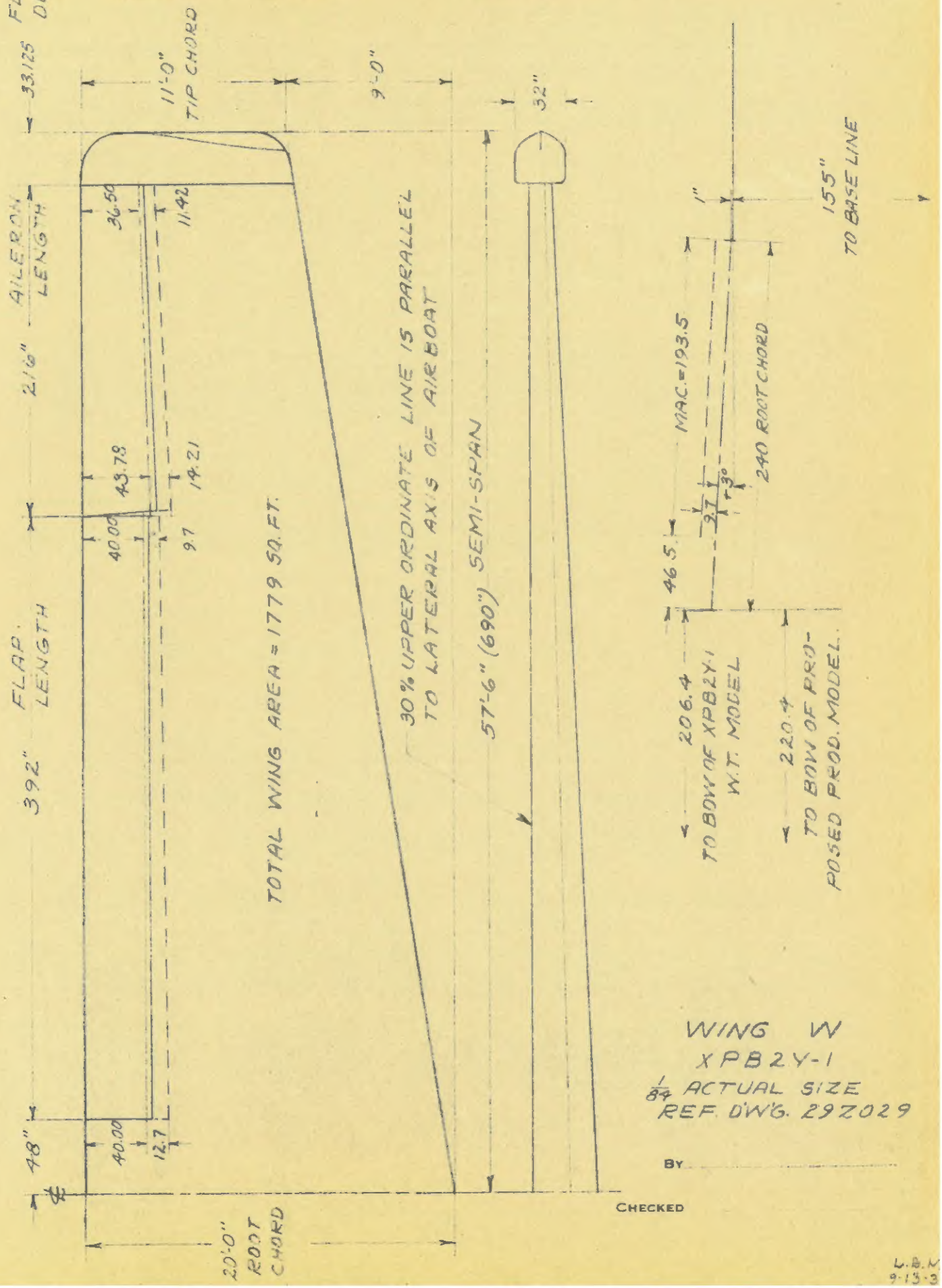

WING W
XPB2Y-1
1/84 ACTUAL SIZE
REF. DWG. 29Z029

BY

CHECKED

L.B.K
9-13-3